İSTANBUL UNIVERSITY CERRAHPAŞA

RESEARCH ARTICLE

Electrica 2020; 20(1): 41-51

Design of a MEMS-Based Capacitive Resonator for Target Analyte Detection

Serdar Tez[1], Ergun Aytaşkın[2]

[1]Department of Electrical and Electronics Engineering Pamukkale University Faculty of Engineering, Denizli, Turkey
[2]Department of Electrical and Electronics Engineering, Pamukkale University, Graduate School of Natural and Applied Sciences, Denizli, Turkey

Cite this article as: Tez S, Aytaşkın E. Design of a MEMS-Based Capacitive Resonator for Target Analyte Detection. *Electrica*, 2020; 20(1): 41-51.

ABSTRACT

The present study introduces a microelectromechanical systems (MEMS) capacitive comb-finger resonator designed for the detection of different target analytes by using the detection mechanism based on the resonance frequency shift. This kind of applications is generally needed for a sensing layer capable of absorbing the desired target species in a molecular level, resulting in a change in the mass of the resonator. Therefore, a conceptual fabrication model is also described to form such a layer on the sensor. The dimension of the designed resonator structure is nearly 1766 μm×1998 μm, and the structural thickness of the sensor is planned to be 35 μm thick. Moreover, the design values of rest capacitance and resonance frequency of the structure are nearly 1 pF and 49 kHz, respectively. The inverse of the mass responsivity of the design given in the study is calculated as 370 pg/Hz. In addition to theoretical calculations, the mechanical and electrical simulations are also performed to verify the results.
Keywords: Microelectromechanical systems (MEMS), capacitive resonator, finite element method (FEM), resonance frequency shift, sensor

Corresponding Author:
Serdar Tez

E-mail:
stez@pau.edu.tr

Received: 02.08.2019

Accepted: 01.11.2019

DOI: 10.5152/electrica.2020.19054

Introduction

Microelectromechanical systems (MEMS), which is enabling the machining of silicon in a micro-level, is a growing research interest due to its matchless properties, such as allowing fabrication of sensors with portable, low-power consumption; robust; and cost efficient. There are various sensing mechanisms used in MEMS technology, such as optic [1], piezoresistive [2], surface acoustic wave [3], and resonant-based gravimetric techniques [4]. The resonant-based gravimetric technique is mainly preferred for many sensor implementations due to its high-mass resolution. Furthermore, this method needs not only a special sensing layer but also an actuation mechanism. The special sensing layers, such as polystyrene [5] and PEDOT/PSS [6], are capable of absorbing the desired target species in a molecular level and cause a change in mass, resulting in frequency shift. The capacitive transduction is generally implemented for resonant-based gravimetric sensor applications for actuation mechanism. MEMS cantilever is a popular structure used in resonant-based gravimetric sensor applications in the literature. The microcantilever structure can be modeled as a spring structure extending from a fixed end. The mechanical spring providing the movement of the structure in the vertical direction is also a proof mass for this structure. However, some problems are observed during the fabrication and the functionality test of the microcantilever, such as structural buckling [7], the effect of the thickness and the position of the sensing layer to the output signal of the microcantilever [8], low mechanical quality factor (*Q*—quality factor) [9], and the effect of the different mechanical mods of the microcantilever to the mass sensitivity [10]. Furthermore, depositing the sensing layer to the optimum position on the microcantilever is a challenging problem in the literature [8], causing the position- and thickness-dependent sensing characteristics. Some of these problems can be eliminated by laterally moving resonators already reported in the literature for gravimetric applications [11, 12]; however, these sensors have very thin (~5 μm) structural thickness. Although the mass sensitivity is increased for these sensors, the motional current level is also decreased, and they need high DC bias voltage as a result of using very thin structural thickness. Furthermore, they are not designed for applications

requiring sensing layer and need an effective solution for the formation of sensing layer.

Therefore, the present study combines the mechanical advantages of a laterally moving resonator with easy and effective solution provided by a silicon shadow mask, which will allow to form a sensor having both reliable and independent sensing features compared with the literature. Thus, the proposed sensor structure can be modified for sensing various chemical analytes.

Theory

The MEMS capacitive resonator structure comprises three main parts: proof mass, mechanical springs, and capacitive electrodes. The MEMS resonator structure can be modeled as a mass, spring and damper system. Figure 1a shows the model of the resonator. When an external force is applied, the model of the resonator can be expressed with a second order differential equation given in Eq. (1).

$$m\frac{d^2x}{dt^2} + b\frac{dx}{dt} + kx = F \tag{1}$$

where x is the displacement, b is the damping coefficient, m is the mass of movable body, and k is the mechanical spring constant. By using the Laplace transform for Eq. 1, the transfer function of the system can be obtained and given as Eq. (2).

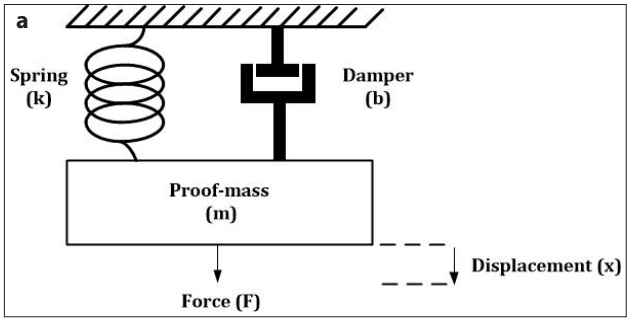

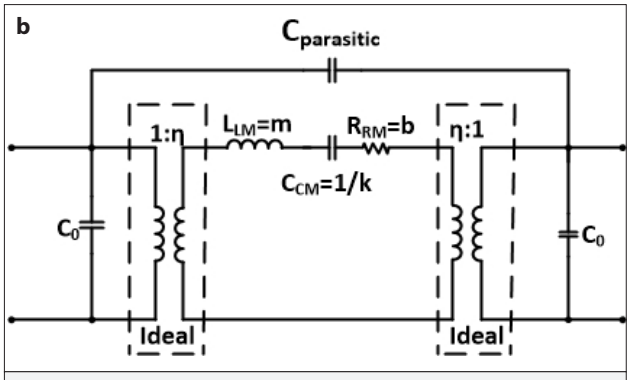

Figure 1. a, b. The mechanical model of the MEMS capacitive resonator (a). The electrical equivalent model of the MEMS capacitive resonator (b)

$$x(s) = \frac{F(s)}{ms^2 + bs + k} \tag{2}$$

The quality factor (Q) and the natural resonance frequency (ω_0) of the system can be determined by arranging Eq. (1), and these expressions are given in Eq. (3).

$$\omega_0 = \sqrt{\frac{k}{m}} \qquad Q = \frac{\omega_0 m}{b} \tag{3}$$

The spring constant and damping coefficient shown in Figure 1a are based on the design of the structure. The folded beam structure is generally preferred for the mechanical springs, and the spring constant of the resonator can be calculated as Eq. (4)

$$k = \frac{Ehw^3}{l^3} \tag{4}$$

where E is the Young's modulus and h, w, and l are the structural thickness, the width, and the length of the mechanical spring structures, respectively.

On the other hand, the damping coefficient depends on several parameters, such as the material used during the fabrication of the microstructure, the mechanical boundary condition, and the fluid medium [13]. Especially, when the microstructure operates in the surrounding air medium, there are two major damping mechanisms, squeeze film air damping [14] and slide film air damping [15]. Furthermore, the squeeze film air damping has a more dominant characteristic than the slide film damping on the microstructure; however, the calculation of the damping coefficient is rather difficult. Therefore, the effect of the squeeze film air damping can be minimized during the design of the structure by providing a lateral motion with the placement of the springs, allowing the change of the overlap area among the fingers.

The lateral motion of the structure can be provided with the capacitive actuation. The capacitive actuation forms an electrostatic force between the fingers of the proof mass and one of the electrodes to drive the sensor on the desired motion. The electrostatic force equation can be obtained by calculating the gradient of the stored electrostatic energy. The stored electrostatic energy for the parallel plates capacitor is defined in Eq. (5).

$$E = \frac{1}{2}CV^2 \tag{5}$$

where C is the capacitance formed among the fingers of the proof mass and electrodes and V is the electrical potential. The capacitance value given in Eq. (5) can be defined in Eq. (6)

$$C = \frac{\varepsilon_0 A}{d} \tag{6}$$

where ε_0 is the permittivity of the free space, A is the area between the parallel plates, and d is the gap between the capacitive fingers of the proof mass and electrodes. By using Eqs. (5) and (6), the electrostatic force can be given in Eq. (7)

$$F = \frac{1}{2}\frac{\partial C}{\partial x}V^2 \tag{7}$$

where $\partial C/\partial x$ is the partial derivative of Eq. (5) with respect to the x displacement as a result of movement changing the overlap area among the fingers. When the electrical potential including AC and DC components is applied to the proof mass and drive electrode, the electrostatic force is defined in Eq. (8).

$$F = \frac{1}{2}\frac{\partial C}{\partial x}\left[\left(V_{DC}^2 + \frac{V_{ac}^2}{2}\right) + 2V_{DC}V_{ac}\,sin(\omega t) - \frac{V_{ac}^2 cos\,(2\omega t)}{2}\right] \tag{8}$$

Although Eq. (1) defines the dynamic behavior of the system, it is also necessary to model the whole electromechanical system by converting the mechanical parameters to their electrical equivalents. For this conversion, the similarity between the mathematical differential model of a mass–damper–spring system and that of the serial RLC circuit can be used. The mass, damping coefficient, and spring constant correspond to the inductance, resistor, and inverse of the capacitance, respectively, when two differential equations are compared with each other. Figure 1b shows the electrical equivalent circuit model of the resonator, where C_0 is the rest capacitance formed among the capacitive fingers and $C_{parasitic}$ can be defined as the feedthrough capacitance formed between the input and output ports of the circuit. Moreover, it is necessary to use an equivalent conversion coefficient (η) to transform mechanical and electrical parameters to each other. η is given by Eq. (9).

$$\eta = \frac{\partial C_0}{\partial x}V_{DC} \tag{9}$$

By using η, it is possible to express the inductance, resistor, and capacitance of the equivalent electrical circuit using Eq. (10).

$$R_{RM} = \frac{b}{\eta^2} \qquad C_{CM} = \frac{\eta^2}{k} \qquad L_{LM} = \frac{m}{\eta^2} \tag{10}$$

Finally, for the circuit shown in Figure 1b, the motional current as a result of movement of the resonator is defined in Eq. (11).

$$i_m(s) = \eta s x(s) \tag{11}$$

Then, it is possible to use a transimpedance op-amp to convert the motional current to voltage.

The resonator structures are also used for mass-sensing applications. For this case, the mass sensitivity is defined as an expression given in Eq. (12).

$$S = \frac{\delta_f}{\delta_{mass}} \cong \frac{f_0}{2m} \tag{12}$$

where $R = \frac{f_0}{2m}$ is the mass responsivity, δ_{mass} is the added mass and δ_f is the resulting frequency shift.The minimum detectable mass and the minimum detectable frequency expressions are also important parameters in determining the device performance, and they can be obtained by using the equation of the minimum detectable force gradient defined in Eq. (13) [16].

$$\delta F_{min} = \frac{2k\delta\omega}{\omega_o} = \sqrt{\frac{4kk_BT\,B}{\omega_o Q\langle x^2_{amplitude}\rangle}} \tag{13}$$

where $\delta\omega$ is the density of frequency noise, k_B is the Boltzmann constant, T is the temperature, B is the bandwidth, and $x^2_{amplitude}$ is the mean square amplitude of the self-oscillating resonator.

Design

Figure 2 shows the conceptual design of the MEMS resonator. The movable proof mass of the resonator is attached to the anchor regions by using the mechanical spring structures. Therefore, the four mechanical spring structures are placed to the corner of the proof mass region to provide motion in the lateral direction, whereas it prevents the undesired vertical movement. The finger structures are placed side by side in the proof mass and electrode regions, forming an equal capacitance value between the drive electrode and the proof mass, as well as the sense electrode and the proof mass. The proof mass amount is also calculated by using a simple equation between the density of silicon and volume. Table 1 shows the parameters used during the design of the MEMS resonator.

Theoretical Analysis

For the given design values in Table 1, the theoretical calculations are performed for the values of the resonance frequency and the rest capacitance by using Eqs. (3) and (6), respectively. Moreover, the damping coefficient can be calculated by using the equations given in previous studies [14-15]. Then, it is pos-

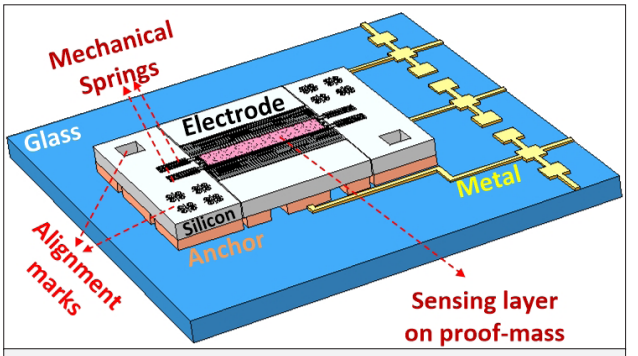

Figure 2. The conceptual design of the MEMS resonator

Table 1. The design parameter of the MEMS resonator

Structural thickness (μm)	35
Spring width (μm)	4
Spring length (μm)	120
No. of spring	4
Spring constant (N/m)	876
Finger width (μm)	4
Finger length (μm)	100
Overlap finger length (μm)	60
Capacitive gap (μm)	2
Capacitive anti-gap (μm)	2
No. of finger per electrode	50
Mass of the proof mass (kg)	9.13×10^{-9}
Inverse of mass responsivity (R^{-1}) (pg/Hz)	370

Table 2. The calculated design parameters of the MEMS resonator

Resonance frequency (f_0) (Hz)	49,297.46
Rest capacitance in air medium (pF)	0.919
Effective sensitivity (∂C/∂x) (F/m)	1.53×10^{-8}
Calculated Q	364
Q value used during the design	100
V_{dc} (V)	5
V_{ac} (V)	0.75 sinωt

Table 3. The comparison of the obtained results

Results	**Theoretical**	**Simulation**
1st mode resonance frequency (kHz)	49.297	46.058
2nd mode frequency (kHz)	–	167.782
3rd mode frequency (kHz)	–	205.167
Rest capacitance (pF)	0.919	1.08

sible to calculate *Q* value by using Eq. (3). However, it is rather difficult to estimate the damping coefficient.

Some of the studies [17] show that the *Q* value of the resonator operating in air is in the range of approximately 100. Therefore, this value can be used to extract the other parameters depending on the *Q* value. Table 2 shows the results of theoretical calculation. The dynamic behavior of the system is analyzed by using Eq. (2), and displacement *x* is obtained with respect to the frequency for different *Q* values. Figure 3a shows the obtained results for these calculations. It is also possible to examine the parameters, such as the capacitance, the minimum detectable mass, and the minimum detectable frequency by using different *Q* values with respect to the frequency. Figure 3b–d shows the graphics of the mentioned parameters. The obtained values of the minimum detectable frequency and the minimum detectable mass are theoretical limits, and they are calculated by taking into account only the effect of thermal noise. However, it should be noted that the electronic noise is also another important parameters limiting the values of these parameters. The values of the minimum detectable frequency and the minimum detectable mass are nearly 0.02 Hz and 7.18 pg for *Q*=100, respectively, when the graph is examined.

Mechanical Simulation Results

An open-source multiphysics simulation program ELMER [18] depending on the finite element method (FEM) is used to verify the design parameters of the MEMS resonator. A three-dimensional (3D) model of the MEMS resonator structure is constructed by using a computer-aided design program. Then, this model is transferred to the ELMER FEM to perform the modal analysis of the structure. During simulation, the structure is fixed in certain regions, and then the mesh settings should be carefully selected not only to attain the optimum results but also to reduce the computational duration. After the simulation is completed, the visualization of the simulation result is performed by using ParaView [19]. Figure 4a shows the analysis result of the MEMS resonator. It can also be seen in Table 3 that the resonance frequency values of the higher-order modes are highly different from those of the first mode, which is necessary for safe operation. Furthermore, the theoretical calculation value is in good agreement with that of the simulation result. However, the reason of slight difference is related with value of the effective mass which corresponds to the whole moving body. A capacitive analysis is also performed through the ELMER FEM for the designed MEMS resonator to verify the theoretical calculation. Thus, another 3D model is also constructed for the region among the fingers. The constructed 3D model is again transferred to the ELMER FEM, and then the rest capacitance value is determined as 1.08 pF for the air medium. The visualization of the electrical potential is performed by using ParaView [19]. Figure 4b shows the result of the simulation. The simulation result is very close that of the theoretical calculation; however, the fringing field is the reason of the slight difference between the obtained results.

Electrical Equivalent Circuit Simulation

The electrical equivalent circuit can be formed by using Eq. (10). When Eq. (10) is examined, L_{LM} and C_{CM} are mainly dealt with the mass and mechanical spring constant of the proposed MEMS resonator, whereas R_{RM} has a close relationship with the damping coefficient. The other characteristic parameter on the electrical equivalent circuit is η, and it can be changed with respect to the different DC bias voltage values. The values of the L_{LM} and C_{CM} are determined for 5 V DC bias voltage value, and

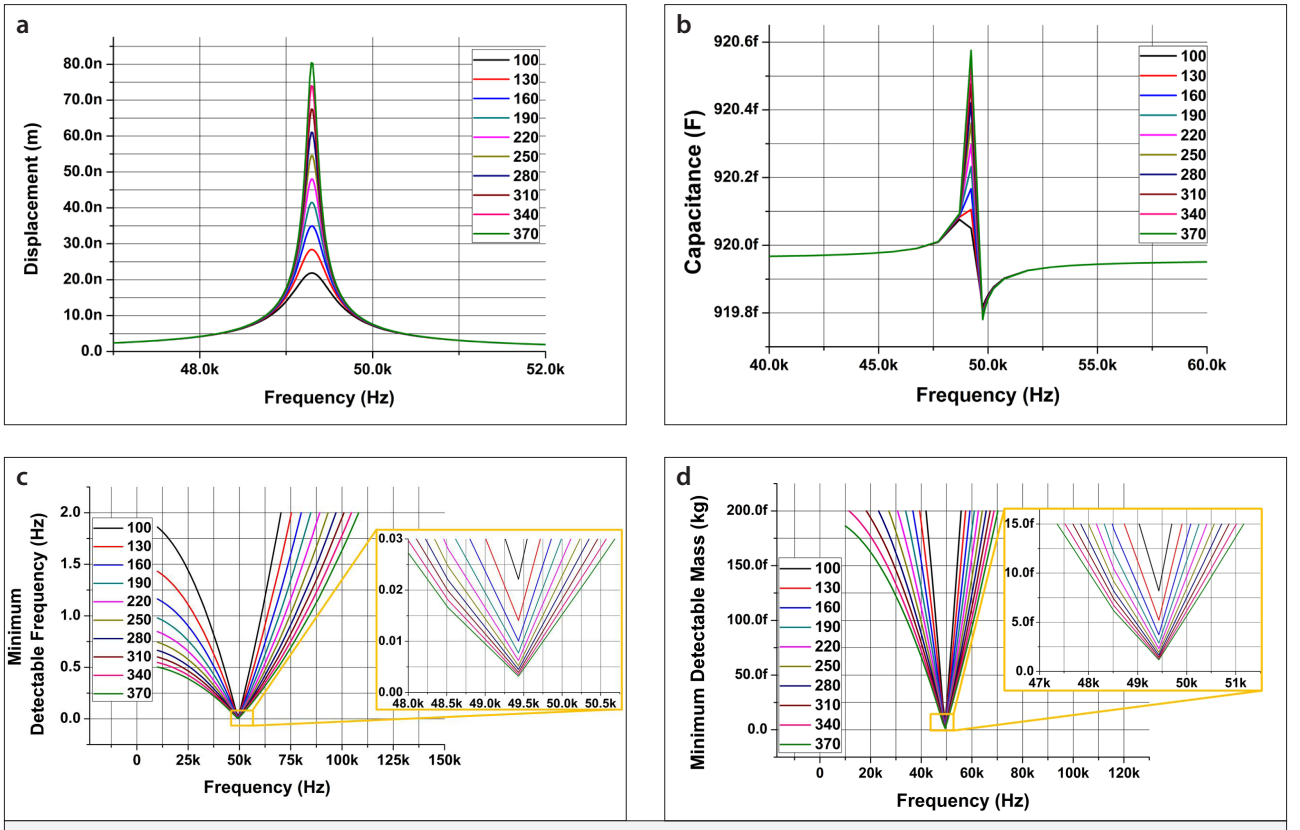

Figure 3. a-d. Graphs of displacement versus frequency (a), rest capacitance versus frequency (b), minimum detectable frequency versus frequency (c), and minimum detectable mass versus frequency obtained for the different Q values (d)

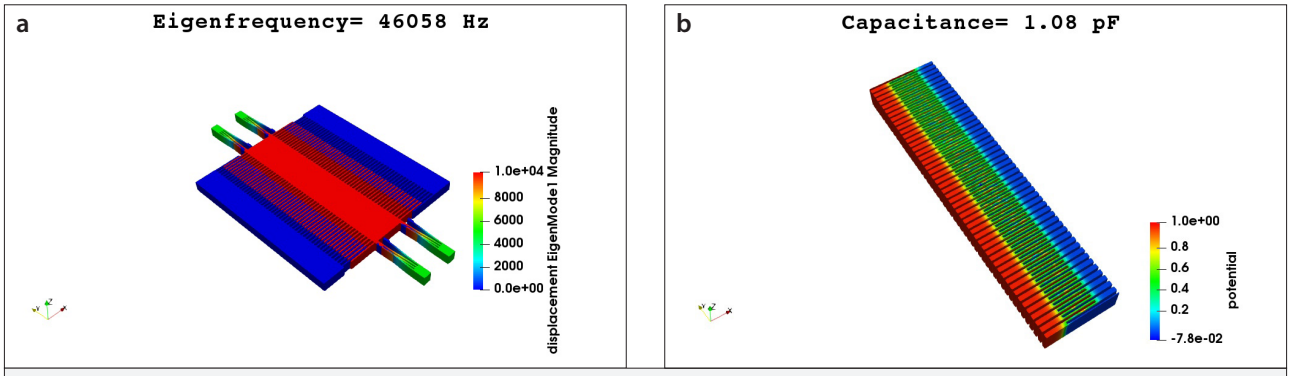

Figure 4. a, b. The modal analysis simulation result (a). The simulated capacitance value (b)

several resistor R_{RM} values are obtained with respect to different quality factor values corresponding to overdamped (for $Q=1/3$, R_{RM} = 1444.09 GΩ), critically damped (for Q=0.5, R_{RM} = 962.72 GΩ), and underdamped characteristics (for Q=1, R_{RM} = 481.36 GΩ), as well as for selected design value Q=100, R_{RM}=4.81 GΩ). Table 4 shows the obtained values of the electrical equivalent circuit. After determining the equivalent circuit parameters, a transient analysis is performed for the equivalent series RLC circuit by using an AC pulse source providing 0.75 V and different resistor values. Figure 5a shows the response of the equivalent series RLC circuit with respect to the obtained resistor values. Furthermore, some of the parameters for the electrical equivalent circuit are calculated, such as Neper frequency α, damping factor ξ, and the natural resonance frequency and given in Table 5 for selected design value Q=100. Moreover, the circuit is integrated with a transimpedance op-amp (TI OPA 656, Texas Instruments, Dallas, TX, USA) and a feedback resistor with 1 MΩ value to convert motional current to voltage. Then, the simulation is performed by using a SPICE simulation program. Figure 5b shows the simulation result for gain and phase response of the equivalent circuit with respect to the frequency, whereas the feedthrough capacitance $C_{parasitic}$ is ignored. The transient

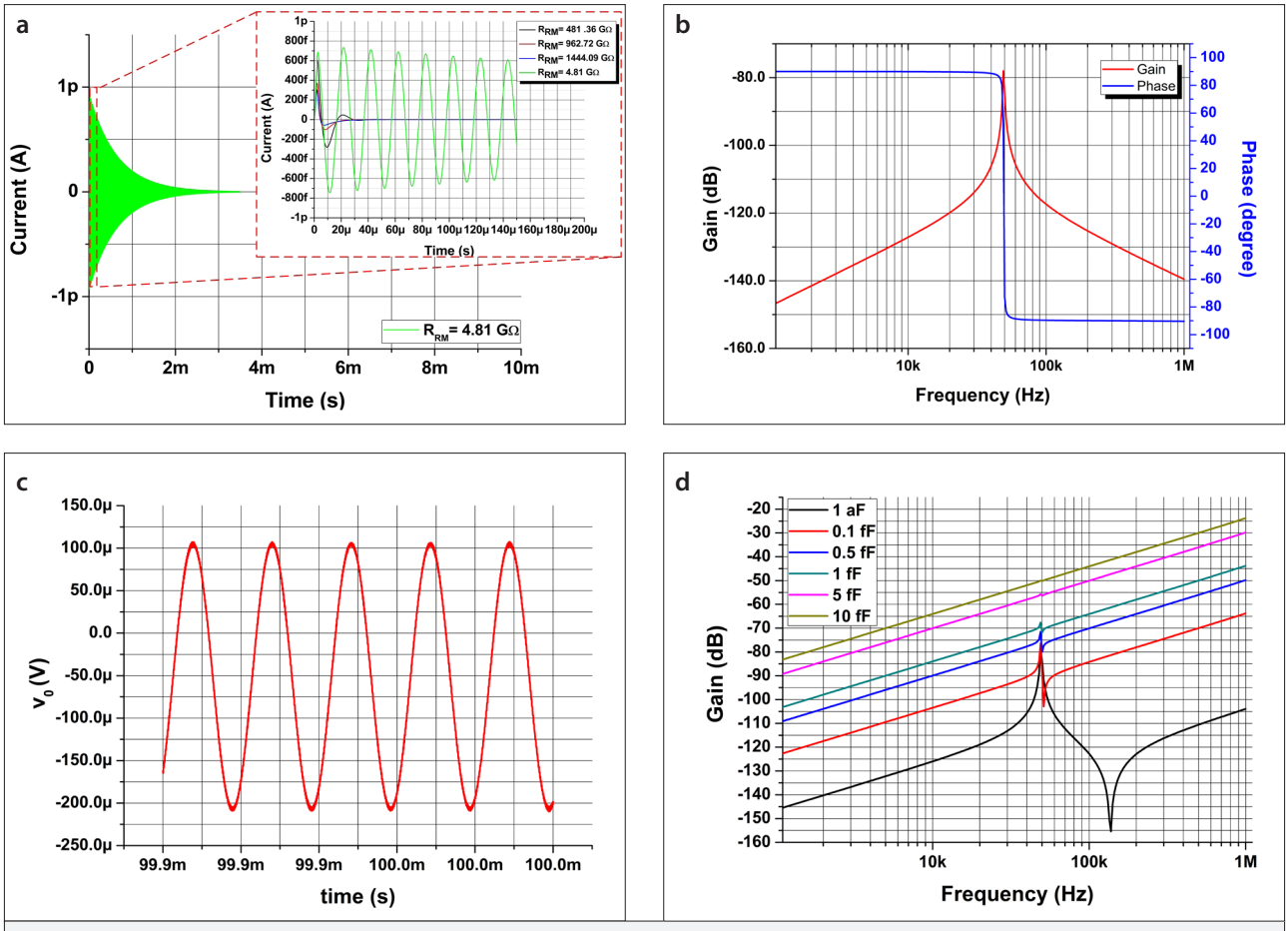

Figure 5. a-d. The transient analysis result for the series RLC circuit (a). The simulated responses of the equivalent circuit (b, c). The effect of the different parasitic capacitance $C_{parasitic}$ values to the gain response of the sensor (d)

Table 4. The equivalent circuit parameters for different DC bias voltage values

Parameters	Value for 5 V
L_{LM} (H)	1.55 M
R_{RM} (Ω) (for Q=100)	4.81 G
C_{CM} (F)	6.7 a
C_0 (F)	0.919 p

Table 5. Some of the parameters for the equivalent series RLC circuit

Parameters	Values
α (rad/s)	~1550
ξ	~5×10^{-3}
Natural resonance frequency (Hz)	49,298.26

analysis is also performed for this circuit, and the simulation result is given in Figure 5c. The parasitic feedthrough capacitance formed between the drive and sense port deteriorates the gain response of the sensor, and it is difficult to observe the resonance peak of the sensor as its value increases. Figure 5d shows such an analysis for the designed MEMS capacitive resonator for the different values of $C_{parasitic}$.

Proposed Fabrication Method

There are several fabrication methods for the MEMS sensor structures presented in the literature, such as the Dissolved Wafer Process [20] and the Modified-Silicon-on-Glass fabrication process (M-SOG) [21, 22]. The proposed MEMS capacitive sensor structure can be fabricated by using one of the mentioned fabrication methods. The M-SOG fabrication process is preferred among these fabrication methods due to forming low parasitic capacitance and high yield. Therefore, a three-layer fabrication mask set is designed for the formation of the structure on the silicon layer and the anchor region on the glass substrate, as well as the metal pads. Figure 6 shows the fabrication mask set for the MEMS resonator. The designed mask set is also compatible to use in different fabrication methods mentioned above. Furthermore, a shadow mask is designed to integrate

Table 6. Comparison of the resonator structures used in mass-sensing applications

Ref.	Type and size of the sensor	Detection method	Operation mode	Frequency (Hz)	Q in air medium	Min. Δf (Hz)	Type of sensing element	Target analyte and sense amount	Detection time
[5]	Micromechanical oscillator Beam size *l*=120.6 µm *w*=1.8 µm *h*=4.9 µm Plate size 116 µm×103 µm *h*=1 µm	Electrostatic actuation/ capacitive detection	Lateral	5.475 k	NA	NA	Polystyrene	Methanol 193.5 pg, ethanol 188.8 pg, 2-propanol 122.7 pg, acetone 606.5 pg	~6 min (steady state)
[11]	MEMS comb-finger *h*=5 µm	Electrostatic actuation/capacitive detection	Lateral	~1.98 M~ 558 k	1800 350	NA	NA	Beads 5.91 fg/Hz	NA
[12]	MEMS comb-finger *h*=5 µm	Electrostatic actuation/capacitive detection	Lateral	~245 k	NA	NA	NA	Beads 588 fg/Hz	NA
[23]	NEMS cantilever *l*=40 µm *w*=840 nm *h*=600 nm	Electrostatic actuation/capacitive detection	Lateral	703 k	21	1.9	NA	NA Expected limit of detection ~65 ag	NA
[24]	NEMS cantilever *l*=10 µm *w*=600 nm *h*=750 nm	Electrostatic actuation/capacitive detection	Lateral	~6 M	100	NA	NA	NA Expected limit of detection ~1.4 ag	NA
[25]	20 µm long microcantilever composed of two sidewalls with *w*=1.2 µm *h*=4.5 µm bounded with a channel *w*=2.1 µm *h*=1.7 µm	Electrostatic actuation/capacitive detection	Twist	206.6 k	NA	NA	poly (butylmethacrylate) (PBMA)	Toluene 1.6 ppm, Acetone 5.5 ppm, Methanol 16 ppm	NA
[26]	Microcantilever *l*=1500 µm *w*=100 µm *h*=300 µm	Piezoelectric/ resonance shift	Flexural vibration mode	341 k	71	NA	poly methyl methacrylate (PMMA) cantilever and piezoelectric film of polyvinylidene fluoride (PVDF) and a thin film of polybutadiene (PBD)	Toluene 0.02 Hz/ppm	1 min

Table 6. Comparison of the resonator structures used in mass-sensing applications (Continue)

Ref.	Type and size of the sensor	Detection method	Operation mode	Frequency (Hz)	Q in air medium	Min. Δf (Hz)	Type of sensing element	Target analyte and sense amount	Detection time
[27]	Resonant micro-structure formed by a semicircular head with 200 µm outer radius and 75 µm wide and 100 µm long cantilever	U-shaped Wheatstone bridge/ resonance frequency shift	In-plane resonance mode	780 k	2000	NA	Polyisobuty-lene (PIB)	Toluene fre-quency drop of ~1.2 kHz	NA
[28]	Resonant cantile-ver, capacitive sensor	Piezoresistive Wheatstone bridge/capaci-tance change	In-plane resonance mode	375 k	NA	NA	Amino-functionalized sensing film	CO	NA
[29]	Microcantilever integrated with suspended micro-channel	Piezoresistive sensor/frequen-cy shift	NA	95.7 k (max)	415 (max)	NA	NA	Air particle 0.227 Hz/pg	NA
This study	MEMS comb-finger Die size 1766×1998 µm^2 h=35 µm	Electrostatic ac-tuation/capaci-tive detection	Lateral	49 k	Expected 100	Theo. limit 0.02	Customizable	Customizable theoretical R^{-1}= 370 pg/Hz	NA

NA: not available

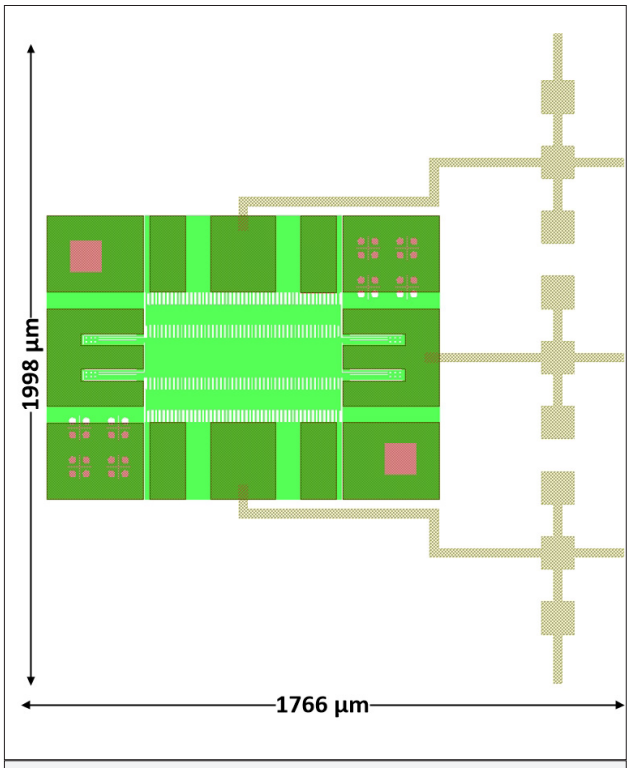

Figure 6. The fabrication mask set for the MEMS resonator

any sensing layers with the proof mass of the MEMS resonator, ensuring the position-independent sensing characteristic. Such a mask can be formed by using the fabrication flows defined in Figure 7a. First, the front side of the <100> silicon wafer with 500 µm thick is coated with the SiO_2 layer by using plasma-enhanced chemical vapor deposition (PECVD) (Figure 7(i)). Then, the silicon wafer is etched in potassium hydroxide (KOH) solution to thin the wafer until 300 µm (Figure 7(ii)). The next step is to deposit the SiO_2 layer by using PECVD (Figure 7(iii)) to the rear side of the wafer. The lithography processes are performed for the patterning and developing of the photo-resist. Then, the SiO_2 layers are etched by using buffered hydro-fluoric acid (BHF) (Figure 7(iv)). Next, the silicon wafer is etched by using deep reactive ion etching (DRIE) (Figure 7(v)), and the SiO_2 layer is etched by using BHF (Figure 7(vi)). Finally, the fab-ricated sensor wafer and the silicon shadow mask wafer can be aligned to deposit the sensing layer by using air brush or spray coating. Figure 7b shows the conceptual model. The formation of both the wafer level and die level alignment marks will help the deposition of the sensing layer. Table 6 shows a comparison for the proposed MEMS resonator and the different sensors al-ready reported in the literature with respect to the type of the device and the other performance parameters.

When preliminary results given in the present study are taken into account, the proposed MEMS resonator is mainly different

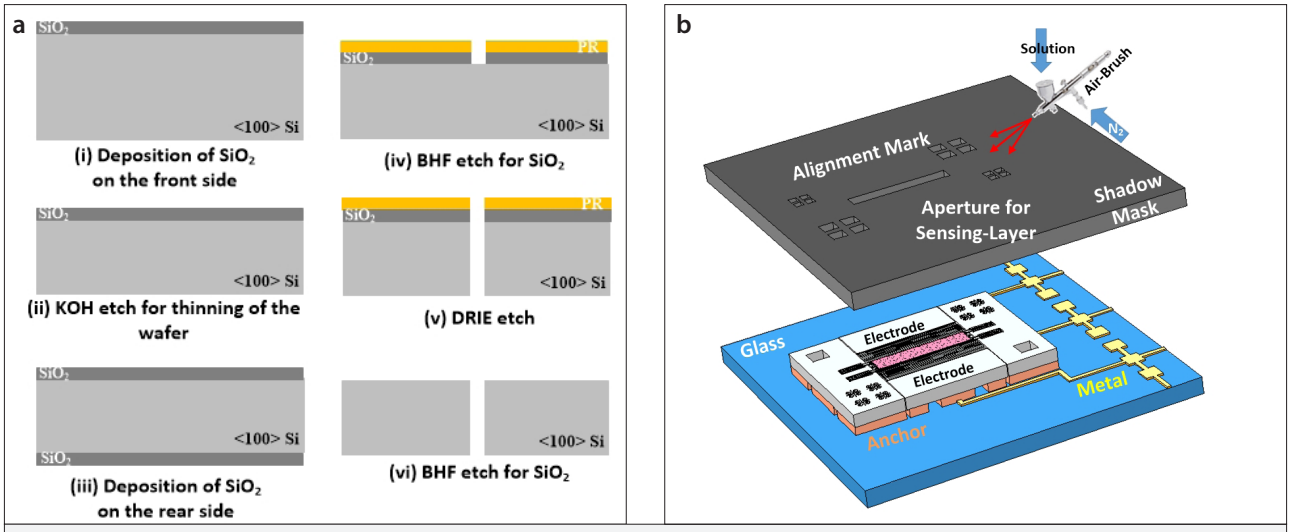

Figure 7. a, b. (a) The fabrication process flow for the silicon shadow mask. The conceptual design of the sensor (b)

from the literature as a result of using the comb-drive structure for mass-sensing applications and having a fabrication process allowing the formation of the specific sensing element for target analytes. Furthermore, the proposed sensor integrates the mechanical advantages of the comb-drive resonator with easy and effective solutions to modify the sensing layer for different applications. Especially, the implementation of the proposed sensor can be expanded to chemical gas sensing applications. For this application, it is also possible to integrate the proposed sensor with both commercial polymers, such as polystyrene and PEDOT/PSS, as well as specially designed conducting polymers [30].

Conclusion

The present study presents a MEMS comb-finger structure which can be used for the detection of various analytes with the help of the proposed fabrication processes. The resonance frequency of the sensor can be increased by not only changing the size of the spring structures but also decreasing the amount of the proof mass at the expense of using higher DC bias voltage during the operation.

The present study introduces a conceptual method to design and fabricate a customizable MEMS capacitive resonator. The proposed MEMS resonator can be a good candidate for the detection of volatile organic chemicals which is a biomarker for several diseases and threaten the indoor air quality.

Peer-review: Externally peer-reviewed.

Acknowledgements: The authors would like to thank to the Scientific and Technological Research Council of Turkey (TUBITAK). The authors would also like to thank to Prof. Dr. Metin AK for valuable discussion.

Conflict of Interest: The authors have no conflicts of interest to declare.

Financial Disclosure: This work is supported by the Scientific and Technological Research Council of Turkey (TUBITAK) under grant number 116E231.

References

1. Y. Arntz, J. D. Seelig, H. P. Lang, J. Zhang, P. Hunziker, J. P. Ramseyer, E. Meyer, M. Hegner, Ch. Gerber, "Label-free protein assay based on a nanomechanical cantilever array", Nanotechnology, vol. 14, no. 1, pp. 86-90, Dec., 2002. [Crossref]
2. L. G. Carrascosa, M. Moreno, M. Álvarez, L. M. Lechuga, "Nanomechanical biosensors: A new sensing tool", Trends in Analytical Chemistry, vol. 25, no. 3, March, 2006. [Crossref]
3. M. C. Horrillo, M. J. Fernández, J. L. Fontecha, I. Sayago, M. García, M. Aleixandre, J. P. Santos, L. Arés, J. Gutiérrez, I. Gràcia, C. Cané, "Detection of volatile organic compounds using surface acoustic wave sensors with different polymer coatings", Thin Solid Films, vol. 467, no.1-2, pp. 234-8, Nov., 2004. [Crossref]
4. Y. Dong, W. Gao, Q. Zhou, Y. Zheng, Z. You, "Characterization of the gas sensors based on polymer-coated resonant microcantilevers for the detection of volatile organic compounds", Analytica Chimica Acta, vol. 671, no. 1-2, pp. 85-91, June 2010. [Crossref]
5. S. S. Bedair, Gary K. Fedder, "CMOS MEMS Oscillator for Gas Chemical Detection", IEEE Sensors 2004, Vienna, Austria, 2004, pp. 955-958.
6. B. Charlot, G. Sassine, A. Garraud, A. Giani, P. Combette, "Micropatterning and casting PEDOT-PSS/DMSO layers", Symposium on Design, Test, Integration and Packaging of MEMS/MOEMS, Cannes, France, 2012, pp. 196-9.
7. K. Khosraviani, A. M. Leung, "Stress anisotropy compensation of the sputter-deposited metal thin films by variable bias voltage", J Micromech and Microeng, vol. 23, no. 8, pp. 085005 (7pp), June, 2013. [Crossref]
8. B. N. Johnson, R. Mutharasan, "Biosensing using dynamic mode cantilever sensors: A review", Biosen and Bioelect, vol. 32, no. 1, pp. 1-18, Feb., 2012. [Crossref]
9. A. Mehta, S. Cherian, D. Hedden, T. Thundat, "Manipulation and controlled amplification of Brownian motion of microcantilever sensors", Appl Phys Lett, vol. 78, no. 11, pp. 1637-9, March, 2001. [Crossref]
10. T. Ikehara, J. Lu, M. Konno, R. Maeda, T. Mihara, "A high quality-factor silicon cantilever for a low detection-limit resonant mass sensor operated in air", J Micromech Microeng, vol. 17, no. 12, pp. 2491-4, Nov., 2007. [Crossref]

11. E. Bayraktar, D. Eroglu, A. T. Ciftlik, H. Kulah, "A MEMS based gravimetric resonator for mass sensing applications", IEEE 24th International Conference on Micro Electro Mechanical Systems, Cancun, Mexico, 2011, pp. 817-20. [Crossref]
12. D. Eroglu, E. Bayraktar, H. Kulah, "A laterally resonating gravimetric sensor with uniform mass sensitivity and high linearity", 16th Int Solid-State Sensors, Actuators Microsystems Conference, Beijing, China, 2011, pp., 2255-8. [Crossref]
13. M. Vagia, A. Tzes, "A literature review on modeling and control design for electrostatic microactuators with fringing and squeezed film damping effects", 2010 American Control Conference, Baltimore, MD, USA, 2010, pp. 3390-402. [Crossref]
14. M. Bao, H. Yang, "Squeeze film air damping in MEMS", Sensors and Actuators A: Physical, vol. 136, no. 1, pp. 3-27, May, 2007. [Crossref]
15. W. Wang, J. Jia, J. Li, "Slide film damping in microelectromechanical system devices", Proceedings of the Institution of Mechanical Engineers, Part N: Journal of Nanoengineering and Nanosystems, vol. 227, no. 4, pp. 162-70, August, 2013. [Crossref]
16. T. R. Albrecht, P. Grütter, D. Horne, D. Rugar, "Frequency modulation detection using high-Q cantilevers for enhanced force microscope sensitivity", Journal of Applied Physics, vol. 69, no. 2, pp. 668-73, Jan., 1991. [Crossref]
17. W. C. Chen, W. Fang, S. S. Li, "A generalized CMOS-MEMS platform for micromechanical resonators monolithically integrated with circuits", J Micromech Microeng, vol. 21, no. 6, pp. 065012 (15pp), May, 2011. [Crossref]
18. P. Råback, M. Malinen, J. Ruokolainen, A. Pursula, T. Zwinger, Eds. (May, 2019). Elmer Models Manual. CSC-IT Center for Science.
19. James Ahrens, Berk Geveci, Charles Law, "ParaView: An End-User Tool for Large Data Visualization", Visualization Handbook, 1st Ed., Elsevier, 2005, ch. 36, pp. 717-31. [Crossref]
20. Steve T. Cho "Batch-dissolved wafer process for low-cost sensor applications", Proc SPIE Micromachining and Microfabrication Process Technology, vol. 2639, Sept., 1995.
21. M. M. Torunbalci, E. Tatar, S. E. Alper, T. Akin, "Comparison of two alternative silicon-on-glass microfabrication processes for MEMS inertial sensors", Eurosensors XXV, Athens, Greece, 2011, pp. 900-3. [Crossref]
22. S. Tez, T. Akin, "Comparison of two alternative fabrication processes for a three-axis capacitive accelerometer", Procedia Engineering, vol. 47, pp. 342-5, 2012. [Crossref]
23. J. Verd, G. Abadal, J. Teva, M. V. Gaudo, A. Uranga, X. Borrise, F. Campabadal, J. Esteve, E. F. Costa, F. Perez-Murano, Z. J. Davis, E. Forsén, A. Boisen, N. Barniol, "Design, Fabrication, and Characterization of a Submicroelectromechanical Resonator with Monolithically Integrated CMOS Readout Circuit", Journal of Microelectromechanical Systems, vol. 14, no. 3, pp. 508-19, June, 2005. [Crossref]
24. J. Verd, U.G. Abadal, J. L. Teva, F. Torres, J. Lopez, F. Perez-Murano, J. Esteve, N. Barniol, "Monolithic CMOS MEMS Oscillator Circuit for Sensing in the Attogram Range", IEEE Electron Device Letters, vol. 29, no. 2, pp. 146-8, Feb., 2008. [Crossref]
25. K. L. Dorsey, S. S. Bedair, G. K. Fedder, "Gas chemical sensitivity of a CMOS MEMS cantilever functionalized via evaporation driven assembly", J Micromech Microeng vol. 24, no. 7, pp. 075001 (8pp), May, 2014. [Crossref]
26. N. Shiraishi, M. Kimura, Y. Ando, "Development of PMMA-based gas sensor and its evaluation using a VOC dilution flow system", Microelectronic Engineering, vol. 119, pp. 115-21, May, 2014. [Crossref]
27. C. Carron, P. Getz, S. M. Heinrich, F. Josse, O. Brand, "Cantilever-based resonant microsensors with integrated temperature modulation for transient chemical analysis", 18th International Conference on Solid-State Sensors, Actuators and Microsystems (Transducers 2015), Anchorage, Alaska, USA, 2015, pp. 1511-4. [Crossref]
28. C. Kim, P. Getz, M. G. Kim, O. Brand, "Room-Tempearutre CO2 Sensing Based on Interdigitated Capacitors and Resonant Cantilevers", 19th International Conference on Solid-State Sensors, Actuators and Microsystems (Transducers 2017), Kaohsiung, Taiwan, 2017, pp. 1532-5. [Crossref]
29. Y. Bao, S. Cai, H. Yu, T. Xu, P. Xu, X. Li, "Resonant-gravimetric particle sensors with air-filtering cantilever fabricated in low-cost non-SOI silicon", IEEE Micro Electro Mechanical Systems (MEMS 2018), Belfast, Northern Ireland, UK, 2018, pp. 908-11. [Crossref]
30. T. Soganci, H.C. Soyleyici, M. Ak, "A soluble and fluorescent new type thienylpyrrole based conjugated polymer: Optical, electrical and electrochemical properties", Physical Chemistry and Chemical Physic 18, 14401, 2016. [Crossref]

Serdar Tez received the B.S and the M.S. degrees in the Physics Department from the Süleyman Demirel University, Isparta, Turkey, in 2004 and 2006, respectively. He joined the METU-MEMS Research and Applications Center in 2008. He received the Ph.D. degree in the Micro and Nanotechnology Graduate Program from the Middle East Technical University (METU), Ankara, Turkey, in 2014, with the work on MEMS capacitive three-axis accelerometers. Currently, he is with the Department of Electrical and Electronics Engineering, Pamukkale University, Denizli, 20070 Turkey. His current research interests are the design, simulation, and fabrication methods of microstructures.

Ergun Aytaskin received the B.S. degrees in the Electric Electronic Department from the Pamukkale University, Denizli, Turkey, in 2015. Currently, he is a graduate student at Pamukkale University Electric Electronic Department. He works on MEMS Capacitive Sensors. His research interests design and modeling of microsensors and microactuators.